

Quantum error correction and entanglement phase transition in random unitary circuits with projective measurements

Soonwon Choi,^{1,*} Yimu Bao,^{1,*} Xiao-Liang Qi,² and Ehud Altman^{1,3}

¹*Department of Physics, University of California Berkeley, Berkeley, CA 94720, USA*

²*Stanford Institute for Theoretical Physics, Stanford University, Stanford, CA 94305, USA*

³*Materials Science Division, Lawrence Berkeley National Laboratory, Berkeley, CA 94720, USA*

We analyze the dynamics of entanglement entropy in a generic quantum many-body open system from the perspective of quantum information and error corrections. We introduce a random unitary circuit model with intermittent projective measurements, in which the degree of information scrambling by the unitary and the rate of projective measurements are independently controlled. This model displays two stable phases, characterized by volume law and area law of the steady state entanglement entropy, respectively. The transition between the two phases is understood from the point of view of quantum error correction: the chaotic unitary time evolution protects quantum information from projective measurements that act as errors. A phase transition occurs when the rate of errors exceeds a threshold that depends on the degree of information scrambling, which is estimated by the quantum decoupling theorem in a strong scrambling limit. We confirm these results using numerical simulations and obtain the phase diagram of our model.

A generic unitary evolution of a quantum many-body system scrambles information. Any local degrees of freedom that are initially in an unentangled state become increasingly more entangled with the rest of the system, making the information encoded in them effectively unrecoverable [1–3]. The scrambling dynamics [4–7], evidenced by the growth of the entanglement entropy toward an extensive value [8–11], underlies the rich complexity of quantum dynamics and the fact that simulating it is beyond the capability of classical computers.

In a realistic system, however, unitary dynamics is often interspersed by occasional projective measurements of local observables made by external observers either controlled or accidental. This process disentangles the measured degrees of freedom from the rest of the system, which may reduce the entanglement entropy. Thus, it is natural to ask under what conditions the growth of entanglement is tamed to a point allowing efficient classical simulations of the quantum dynamics [12].

This question has been addressed in a number of recent works. In the special case of non-interacting fermions, quantum states with volume scaling entanglement (volume-law phase) are unstable to any vanishingly small rate of measurement, leading to steady states in which the entropy only scales with the boundary area of a region (area-law phase) [13]. However, the corresponding behavior in generic interacting systems appears to be much more subtle and has not been fully understood. On the one hand, Ref. [14] proposed an approximate hydrodynamic description of the entanglement growth, which implies that any nonzero measurement rate leads to an area-law phase, as in the case of free fermions. On the other hand, two other papers [15, 16] gave opposing arguments, as well as numerical evidence, suggesting a potential transition between two distinct phases: the system remains stable in the volume-law phase for a sufficiently small measurement rate, while it undergoes a transition

into an area-law phase as the rate exceeds a certain critical value.

In this paper, we provide a new interpretation of the entanglement transition using concepts from quantum information theory. This allows us to resolve the controversy between the previous papers and to gain insight on the mechanism that drives the entanglement transition. The existence of a phase transition, or lack thereof, hinges on the nature of the competition between unitary gates and measurements, which may entangle or disentangle different subparts of a system, respectively. The argument in Ref. [14] on the instability of the volume law phase is based on the observation that this competition is fundamentally not symmetric owing to the nonlocal nature of entanglement. Given a bipartition, a local unitary gate may change the entanglement entropy only when it acts nontrivially across the boundary of two subsystems. Thus, in a single time step, the growth of entanglement entropy is limited by the boundary area of a region. On the other hand, the effect of the projective measurements could be nonlocal: by disentangling all of the measured qubits inside the region, the entanglement entropy can be reduced by an extensive amount. If this is a typical scenario for a state with volume-law entanglement, then projective measurements would always overwhelm the entanglement generation of the unitary evolution and destabilize the volume-law phase. Here, we argue that this is not the case.

Our key observation is that nonlocal effects of sparse measurements are greatly suppressed due to the natural quantum error correction (QEC) property of the scrambling unitary evolution. If quantum information is sufficiently scrambled over a unitary time evolution, correlations between two complementary subsystems are hidden in highly non-local degrees of freedom and cannot be revealed by any local measurements. In such case, sparse local measurements, despite their extensive num-

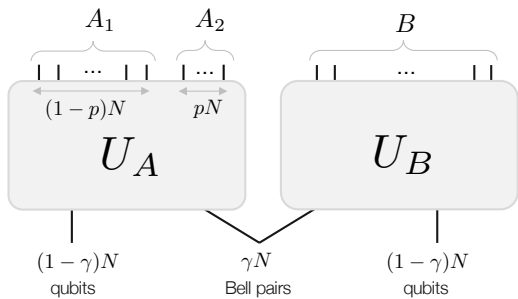


Figure 1. Quantum state of $2N$ qubits generated by applying unitary U_A and U_B to γN Bell pairs. Projective measurements performed on p fraction of qubits (A_2) do not reduce the entanglement between $A = A_1 A_2$ and B as long as $1 - 2p > \gamma$ in the limit $N \rightarrow \infty$.

ber, cannot decrease the entanglement entropy significantly. To illustrate this point and quantify the condition under which the entanglement entropy is robustly protected against local measurements, we apply the quantum decoupling theorem to a specially constructed toy model [17, 18]. We find that the mechanism of the protection is equivalent to that of the QEC scheme developed for quantum communications [17–19]. Motivated by this understanding, we introduce a new model and analyze its dynamics both analytically and numerically to obtain the phase diagram [see Fig. 2(e)]. Our results elucidate the microscopic dynamics of entanglement in open systems, and shows that the stability of the volume-law entangled phase is intimately related to the natural QEC feature of chaotic unitary time evolution.

Protection against measurement.— We now illustrate how entanglement can be protected against measurements using a well-studied toy example from quantum information theory [18, 20–22]. Consider a system of $2N$ qubits ($N \gg 1$) as shown in Fig. 1. Initially, the two halves of the system, A and B , share γN Bell pairs ($0 < \gamma < 1$), which also correspond to the amount of the entanglement between the two. The two subsystems are evolved independently with unitaries U_A and U_B , respectively. We assume U_A is a random unitary drawn from the Haar distribution (or any unitary 2-design), and U_B can be arbitrary. Following this evolution, a fraction p of the qubits in A are measured. The pertinent question to our discussion is by how much these measurements reduce the entanglement between A and B . We shall show that under a certain condition the change of entanglement entropy due to the measurements vanishes in the thermodynamic limit even though an extensive number of qubits are being disentangled.

Let us first simplify the problem slightly. Since U_B does not affect the entanglement, we may simply ignore its effect and replace B with its minimal effective degrees of freedom \tilde{B} entangled with A , i.e., the original γN entangled qubits. Also, we divide A into two parts: subsystem

A_1 refers to the unmeasured qubits and subsystem A_2 contains the measured ones. We now apply the decoupling theorem [18, 20–22] to this setup, which will imply that, for a sufficiently small measurement fraction p , the reduced density matrix of A_2 is effectively decoupled from that of \tilde{B} . More precisely, the decoupling theorem estimates the degree to which the reduced density matrix of A_2 and \tilde{B} factorizes through the inequality

$$\mathbb{E}_U [\|\rho_{A_2 \tilde{B}}(U) - \rho_{A_2}^{\max} \otimes \rho_{\tilde{B}}\|_1] \leq 2^{-(1-2p-\gamma)N/2}. \quad (1)$$

Here, the left-hand side denotes the distance, in the L_1 norm, between the exact density matrix $\rho_{A_2 \tilde{B}}$ and a factorized one, where $\rho_{A_2}^{\max}$ is the maximally mixed state on the measured part A_2 . $\mathbb{E}_U [\cdot]$ represents averaging over the random unitaries drawn from the Haar distribution (or any unitary 2-design).

The inequality implies that the joint quantum state for A_2 and \tilde{B} is approximately factorizable for $N \gg 1$, provided that the number of unmeasured qubits in A is more than half of the total system $A\tilde{B}$:

$$1 - p > \gamma + p. \quad (2)$$

In such cases, any observable in A_2 contains no information about \tilde{B} and vice versa, hence measuring one subsystem does not affect the other up to an error exponentially small in N . In particular, the entanglement entropy of subsystem B is unchanged after the measurements of the qubits in A [23]. In fact, one can show that even the initial γN Bell pairs can be reconstructed by performing only local operations in A_1 with an exponentially good precision [19].

While we considered an ideal situation here—where the Bell pairs are hidden over the entire Hilbert space via a nonlocal unitary—we emphasize that such information scrambling is a generic property of quantum dynamics even in local systems [8–11, 24]. In such cases, we expect that the amount of entanglement reduction is governed by the competition between the rate of effective information scrambling and that of projective measurements.

Model and phase diagram.— Having understood the mechanism to protect the entanglement against projective measurements through scrambling, we turn to study a local 1D model in which the rates of effective information scrambling and projective measurements can be tuned independently. Analyzing this model will result in an interpretation of the entanglement transition as a competition between QEC (by scrambling unitary dynamics) and the loss of information (by projective measurements).

Our model consists of a chain of L blocks, each containing a fixed number ($m \gg 1$) of qubits, as illustrated in Fig. 2(a). In each time step t , the system is evolved by a network of random unitary $U_d(i, t)$ acting on pairs of neighboring blocks at i and $i+1$ (i.e. $2m$ -qubit gates), supplemented by projective measurements. Crucially,

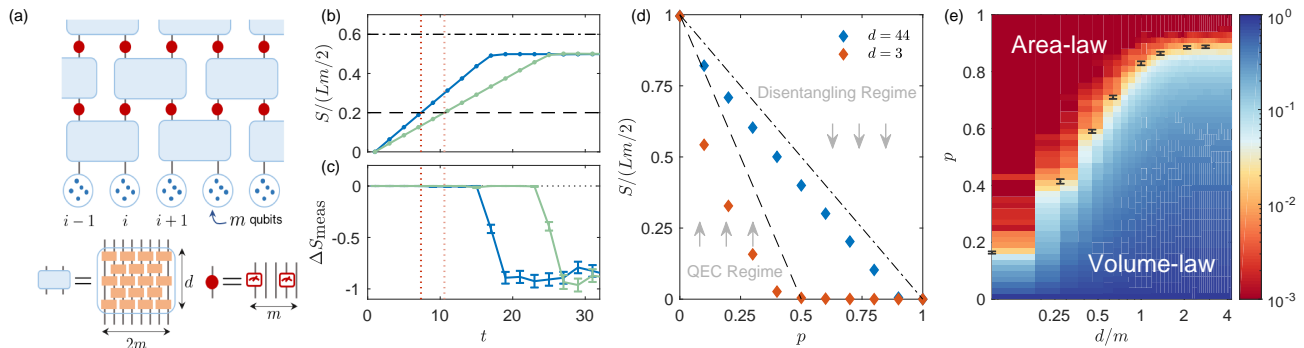


Figure 2. (a) A model with tunable degrees of information scrambling (d) and projective measurements (p). An array of m -qubit blocks undergoes layers of unitary gates (light blue) and random projective measurements (red). Each unitary acting on neighboring clusters comprises a set of independently random 2-qubit gates (orange). Each Measurement projects a randomly chosen fraction p of qubits in each qubit block. (b-e) Numerical simulation results for $m = 11$. (b,c) Entanglement dynamics with $p = 0.4$ for two different system sizes $L = 32$ (blue) and 48 (light green). (b) The growth of entanglement density as a function of time t . (c) The change in the entanglement entropy before and after projective measurements at each time step t . Red dotted lines indicate the regime in which our decoupling inequality is applicable, based on the identification $\gamma = S/(Lm/2)$. (d) Steady state entanglement entropy per qubit as a function of p for two different depth $d = 3$ and 44 . All data are averaged over 240 different realizations of random circuit projective measurements. (e) Phase diagram. When $d \gg m$, the effective quantum error correction protects the volume-law entangled phase from projective measurements up to $p \approx 0.89$ (see main text). The color-coded background displays the half-chain entanglement entropies in steady states, normalized by the number of qubits $Lm/2 = 176$.

the unitary $U_d(i, t)$ are not Haar-random. Instead, they are themselves constructed from an internal network consisting of d layers of independent random 2-qubit gates (over any unitary 2-design). Thus, the parameter d controls the degree of information scrambling within a single $U_d(i, t)$, and, in the limit $d/m \rightarrow \infty$, the distribution of $U_d(i, t)$ can approach a unitary 2-design over $U(2^{2m})$ [24]. After applications of the $U_d(i, t)$ on pairs of blocks, a fraction p of the qubits in each block are randomly chosen to be measured in the computational basis. For non-integer pm , the number of measured qubits is determined from a binomial distribution between $\lfloor pm \rfloor$ and $\lceil pm \rceil$ with mean pm . The measurement process leads to the collapse of the wavefunction, after which the measured qubits are in a product state, completely disentangled from the rest of the system. We note that the special case of our model when $d = 1$ is closely related to the previously studied models in Ref. [14–16]. In particular, according to the argument made in Ref. [14], our model with arbitrary d cannot support the volume-law phase in the thermodynamic limit $L \rightarrow \infty$, since the entanglement entropy across any bipartition may increase at most by $m \log(2)$ while an extensive number of qubits are being measured at every time step.

In our model, the depth d and the fraction p independently control the degree of information scrambling and the measurement rate, respectively. Therefore, we expect a two-dimensional phase diagram, in which the volume-law phase is extended to a larger measurement fraction as d increases. While a quantitative phase diagram can be obtained from numerical simulations as

shown in Fig. 2(e), one can already predict the stability of volume-law phase in the limit $d \gg m \gg 1$ based on the decoupling inequality applied at the microscopic level. More specifically, we consider unitary evolution $U_d(i, t)$ for a single pair of qubit blocks. Identifying the pair of blocks as A and the rest of the system as B , one can use the inequality Eq. (1) similarly to our previous analysis. Then, as long as the average entropy per qubit γ satisfies the criteria in Eq. (2), the measured qubits contain almost no (exponentially small in m) information about the rest of the system. Here, the entanglement reduction is suppressed by information scrambling within the pairs of blocks. Over multiple time steps, quantum information becomes scrambled over a larger region, further protecting the entanglement from projective measurements. In this regime, we expect a stable volume-law phase, where each qubit on average contributes to the global entanglement by γ in the range:

$$1 - 2p \leq \gamma \leq 1 - p. \quad (3)$$

The second inequality is limited by the explicit disentanglement of p fraction of qubits after each measurement step.

We can also make a definitive statement about the other extreme of small d and high measurement rate. Consider, for example the case $d = 1$, $m \gg 1$ and $p = 1 - 1/m$. In this case there is no room for scrambling, thus the probability that a single qubit becomes entangled to other qubits at distance x away (in units of qubit blocks) is exponentially suppressed as $\sim (1/m)^{mx}$ since the information encoded in the qubit needs to prop-

agate without being projected at least $\sim mx$ time steps. This implies the area law entanglement [13]. Thus, we expect a phase transition between the volume law phase, which we know is stable at sufficiently large d and the area law phase we expect to get at $d = 1$ for a high rate of measurements.

In order to verify our theoretical understanding, we numerically simulate the unitary time evolution of our model starting from an initial state $|\Psi_0\rangle = |0\rangle^{\otimes mL}$ and compute half-chain entanglement entropy, $S(t)$, for systems up to 704 qubits and 4247 layers of 2-qubit gates. For our numerical simulations, we assume that each $U_d(i, t)$ is made out of a random 2-qubit Clifford gates drawn from a uniform distribution rather than the Haar distribution. Such $U_d(i, t)$ still approaches a unitary 2-design as d increases [23], hence this simplification does not affect our predictions while allowing for the simulation of substantially larger system sizes [25–28]. Furthermore, the wavefunction evolved under Clifford gates always exhibits a flat entanglement spectrum with respect to any bipartition. Thus, different measures of entanglement entropy, e.g. von Neumann versus Rényi entropies, yield the same value. In the following, our numerical simulations are done with $m = 11$.

We first consider the case $d \gg m$, where the unitary network operating within a single block effectively acts as a random $2^{2m} \times 2^{2m}$ unitary. We can now test if the QEC property of a single block (due to the decoupling theorem applied to it) leads to robustness of the entire circuit. To this end, Fig. 2(b) and 2(c) show the detailed dynamics of the entanglement entropy in the parameter regime, $(p, d) = (0.4, 44)$, averaged over 240 realizations for two system sizes. Clearly, the entropy rescaled by the subsystem size $Lm/2$, exhibits a strict linear growth until it saturates to a constant value. The convergence of this value for different system sizes confirms the volume-law scaling of the entropy in this regime [23]. Moreover we can directly measure how the entanglement entropy changes following the projective measurements in each time step $\Delta S_{\text{meas}}(t)$. The results in Fig. 2(c) show that this change is vanishingly small as long as the entanglement entropy does not exceed a certain threshold. In particular this confirms our prediction that projective measurements do not decrease the entanglement entropy as long as the criterion in Eq. (2) is satisfied [29]. Interestingly, we find the regime of vanishingly small ΔS_{meas} extends even beyond the criterion in Eq. (2). This implies that the inequality in our analysis may not be tight for this particular purpose. Fig. 2(d) shows that the steady state entanglement density, $S/(Lm/2)$, lies within the range defined by Eq. (3) for a large $d = 44$. This is not the case when $U_d(i, t)$ is not sufficiently scrambling, e.g. $d = 3$.

We now turn to the phase transition that occurs when d is decreased (or p is increased). Figure 3(a) shows the scaling of the half-chain entanglement per qubit in the

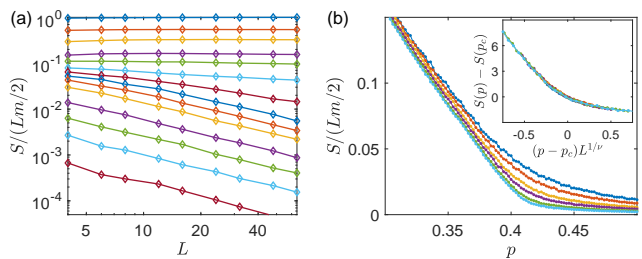


Figure 3. (a) Steady state entanglement density $S/(Lm/2)$ as a function of system size with $m = 11$ and $d = 3$. Different curves from top to bottom represent various measurement fractions p in an increasing order in a range from 0 to 0.9 (unevenly spaced). (b) Finite size scaling analysis of the phase transition. Different curves represent various system sizes $L = 12, 16, 24, 32, 48, 64$. Inset shows the collapse of data with $p_c = 0.41$, $\nu = 1.22$. The data are averaged over 14400 random realizations of unitary circuits and projective measurements.

steady state as a function of system size L for various p with a fixed depth d . For a sufficiently small p , the entanglement density is independent of system size. As we increase p , however, this behavior changes sharply to a linear decrease, $S/(Lm/2) \sim L^{-1}$, indicating an area-law scaling. In order to systematically extract the critical point, we perform a finite size scaling analysis, based on the scaling ansatz proposed in Ref. [30]

$$S(p) - S(p_c) = \mathcal{F}\left((p - p_c)L^{1/\nu}\right), \quad (4)$$

where ν is the critical exponent, p_c is the measurement fraction at the critical point for the phase transition, and $\mathcal{F}(\cdot)$ is a universal scaling function. $S(p_c)$ is the entanglement entropy at the critical point, which is expected to scale logarithmically in L [30]. Repeated over various values of d , we obtain a two-dimensional phase diagram shown in Fig. 2(e). The critical exponent ν has a universal value around 1.1 independent of d which suggests the universality of the transition between two phases [23]. When $d = 1$ the extracted critical value $p_c = 0.16$ is consistent with previous results in Ref. [16, 30]. More importantly, we find that the volume-law entangled phase extends to a higher measurement fraction, as d is increased to $\sim m$, and then saturates for $d \gg m$ where the random unitary U_d approximates unitary 2-design.

Discussions. — The fact that our model exhibits a stable volume-law phase has a direct interpretation in terms of QEC for quantum communications [17], where the primary goal is to devise an encoding scheme to transfer the maximum amount of quantum information over a lossy channel. In fact, one of the most important applications of the decoupling theorem was to show that, by using a random unitary encoding, it is possible to transfer coherent quantum information at an asymptotic rate $1 - 2p$ (number of logical qubits per physical qubit) over a noisy communication channel, while losing a fraction p of the

physical qubits. Here, the coherent quantum information we wish to protect is the entanglement between the qubits encoded by the local random unitary and the rest of the system. In this context, the random unitary circuit in our model is equivalent to repeated encoding of quantum information without explicit decoding. Since this encoding scheme protects $(1 - 2p)2m$ logical qubits in each pair of m -qubit blocks against random measurements in every time step, we expect that our system should exhibit a stable volume-law scaling of the entanglement entropy, supported at least by those logical qubits. This simple analysis provides the lower bound in Eq. (3). We note that this condition is much stronger than what is necessary for a volume-law phase, since the latter only requires protecting total amount of entanglement but not its detailed information such as entanglement spectrum or its basis states (Schmidt states).

An alternative way to analyze the stability of the volume-law phase is to map our model to a classical spin model on a 2D triangular lattice [10]. For example, in the evolution of an initial product state under random unitary circuits *without* measurements, the average Rényi-2 entropy S_2 of any subsystem can be estimated from the partition function of a classical Ising-like model in 2D with appropriate boundary conditions [10], similar to the S_2 calculation of large bond-dimension random tensor networks [31]. This provides a lower bound on the entropy:

$$\mathbb{E}_{U_c} [S_2(t)] \geq -\log(\mathbb{E}_{U_c} [\text{tr}(\rho^2(t))]) = -\log(\mathcal{Z}_{\text{Ising}}), \quad (5)$$

where ρ is the reduced density matrix for a subsystem, $\mathcal{Z}_{\text{Ising}}$ is the partition function of the Ising-like spin model in 2D, and $\mathbb{E}_{U_c} [\cdot]$ indicates the averaging over realizations of random unitary circuit. It can be analytically showed that the average entropy scales with the volume of the subsystem.

In the presence of projective measurements, this approach in general becomes challenging since the measurements give rise to nonlinear transformations of a many-body wavefunction, and the entropy has to be also averaged over different measurement outcomes. In our model, however, these difficulties are significantly alleviated in the leading order in the regime $d \gg m \gg 1$. The decoupling inequality implies that the measurement outcomes are independent and follow a uniform distribution over all possibilities when $p < 1/2$. In this case, the net effect of projective measurements can be approximated by the renormalization of coupling constants in the 2D Ising-like model up to an error that is exponentially small in m .

Summary and outlook.— We introduced a model for a generic open system dynamics with tunable parameters, and demonstrated that this model exhibits two distinct phases with different scaling of entanglement entropy. By using the quantum decoupling theorem, we showed that the volume-law entangled state can be robustly protected against extensive number of measurements via an

effective quantum error correction mechanism naturally realized by the scrambling unitary dynamics. As an extension to this work, it would be interesting to establish general relations between quantum chaos and the stability of the volume-law phase against measurements.

As in the analysis of Refs. [14–16], our analysis focuses on the case of strong projective measurements. It would also be interesting to quantify the protection against continuous weak measurements and identify signatures of the phase transition in properties that may be easier to measure than the entanglement entropy.

Acknowledgements.—We thank X. Chen, Y. Li, I. Kim, A. Nahum, and Q. Zhuang for useful discussions. SC acknowledges support from the Miller Institute for Basic Research in Science. XLQ and EA are supported in part by the Department of Energy project DESC0019380 “The Geometry and Flow of Quantum Information: From Quantum Gravity to Quantum Technology”. EA acknowledges support from the ERC synergy grant UQUAM and from the Gyorgy Chair in Physics at UC Berkeley.

* SC and YB contributed equally to this work.

- [1] J. M. Deutsch, “Quantum statistical mechanics in a closed system,” *Phys. Rev. A* **43**, 2046–2049 (1991).
- [2] Mark Srednicki, “Chaos and quantum thermalization,” *Phys. Rev. E* **50**, 888–901 (1994).
- [3] Marcos Rigol, Vanja Dunjko, and Maxim Olshanii, “Thermalization and its mechanism for generic isolated quantum systems,” *Nature* **452**, 854 (2008).
- [4] Patrick Hayden and John Preskill, “Black holes as mirrors: quantum information in random subsystems,” *Journal of High Energy Physics* **2007**, 120 (2007).
- [5] Yasuhiro Sekino and Leonard Susskind, “Fast scramblers,” *Journal of High Energy Physics* **2008**, 065 (2008).
- [6] Stephen H Shenker and Douglas Stanford, “Black holes and the butterfly effect,” *Journal of High Energy Physics* **2014**, 67 (2014).
- [7] Pavan Hosur, Xiao-Liang Qi, Daniel A Roberts, and Beni Yoshida, “Chaos in quantum channels,” *Journal of High Energy Physics* **2016**, 4 (2016).
- [8] Adam Nahum, Jonathan Ruhman, Sagar Vijay, and Jeongwan Haah, “Quantum entanglement growth under random unitary dynamics,” *Phys. Rev. X* **7**, 031016 (2017).
- [9] CW von Keyserlingk, Tibor Rakovszky, Frank Pollmann, and SL Sondhi, “Operator hydrodynamics, otocs, and entanglement growth in systems without conservation laws,” *Physical Review X* **8**, 021013 (2018).
- [10] Adam Nahum, Sagar Vijay, and Jeongwan Haah, “Operator spreading in random unitary circuits,” *Physical Review X* **8**, 021014 (2018).
- [11] Cheryne Jonay, David A Huse, and Adam Nahum, “Coarse-grained dynamics of operator and state entanglement,” arXiv preprint arXiv:1803.00089 (2018).
- [12] Guifré Vidal, “Efficient simulation of one-dimensional quantum many-body systems,” *Phys. Rev. Lett.* **93**,

- 040502 (2004).
- [13] Xiangyu Cao, Antoine Tilloy, and Andrea De Luca, “Entanglement in a fermion chain under continuous monitoring,” arXiv e-prints , arXiv:1804.04638 (2018), arXiv:1804.04638 [cond-mat.stat-mech].
- [14] Amos Chan, Rahul M. Nandkishore, Michael Pretko, and Graeme Smith, “Weak measurements limit entanglement to area law (with possible log corrections),” arXiv e-prints , arXiv:1808.05949 (2018), arXiv:1808.05949 [cond-mat.stat-mech].
- [15] Brian Skinner, Jonathan Ruhman, and Adam Nahum, “Measurement-Induced Phase Transitions in the Dynamics of Entanglement,” arXiv e-prints , arXiv:1808.05953 (2018), arXiv:1808.05953 [cond-mat.stat-mech].
- [16] Yaodong Li, Xiao Chen, and Matthew P. A. Fisher, “Quantum zeno effect and the many-body entanglement transition,” *Phys. Rev. B* **98**, 205136 (2018).
- [17] Michael A Nielsen and Isaac Chuang, “Quantum computation and quantum information,” (2002).
- [18] John Preskill, “Lecture notes for physics 219: Quantum computation,” (2018).
- [19] Benjamin Schumacher and Michael D Westmoreland, “Approximate quantum error correction,” *Quantum Information Processing* **1**, 5–12 (2002).
- [20] Igor Devetak, “The private classical capacity and quantum capacity of a quantum channel,” *IEEE Transactions on Information Theory* **51**, 44–55 (2005).
- [21] Michał Horodecki, Jonathan Oppenheim, and Andreas Winter, “Quantum state merging and negative information,” *Communications in Mathematical Physics* **269**, 107–136 (2007).
- [22] Anura Abeyesinghe, Igor Devetak, Patrick Hayden, and Andreas Winter, “The mother of all protocols: Restructuring quantum information’s family tree,” *Proceedings of the Royal Society A: Mathematical, Physical and Engineering Sciences* **465**, 2537–2563 (2009).
- [23] See supplementary material online for details.
- [24] Fernando G. S. L. Brandão, Aram W. Harrow, and Michał Horodecki, “Local random quantum circuits are approximate polynomial-designs,” *Communications in Mathematical Physics* **346**, 397–434 (2016).
- [25] Daniel Gottesman, “The heisenberg representation of quantum computers,” arXiv preprint quant-ph/9807006 (1998).
- [26] Scott Aaronson and Daniel Gottesman, “Improved simulation of stabilizer circuits,” *Physical Review A* **70**, 052328 (2004).
- [27] Alioscia Hamma, Radu Ionicioiu, and Paolo Zanardi, “Ground state entanglement and geometric entropy in the kitaev model,” *Physics Letters A* **337**, 22–28 (2005).
- [28] Alioscia Hamma, Radu Ionicioiu, and Paolo Zanardi, “Bipartite entanglement and entropic boundary law in lattice spin systems,” *Physical Review A* **71**, 022315 (2005).
- [29] We note that, for this purpose, we have only considered odd time steps since in even time steps projective measurements destroy local entanglement within the qubit blocks that are generated by immediately preceding $U_d(i, t)$.
- [30] Yaodong Li, Xiao Chen, and Matthew Fisher, “Measurement-driven entanglement transition in hybrid quantum circuits,” arXiv preprint arXiv:1901.08092 (2019).
- [31] Patrick Hayden, Sepehr Nezami, Xiao-Liang Qi, Nathaniel Thomas, Michael Walter, and Zhao Yang, “Holographic duality from random tensor networks,” *Journal of High Energy Physics* **2016**, 9 (2016).

Supplementary Online Material for “Quantum error correction and entanglement phase transition in random unitary circuits with projective measurements”

Soonwon Choi,^{1,*} Yimu Bao,^{1,*} Xiao-Liang Qi,² and Ehud Altman^{1,3}

¹*Department of Physics, University of California Berkeley, Berkeley, CA 94720, USA*

²*Stanford Institute for Theoretical Physics, Stanford University, Stanford, CA 94305, USA*

³*Materials Science Division, Lawrence Berkeley National Laboratory, Berkeley, CA 94720, USA*

(Dated: December 15, 2024)

CONTENTS

S1. Random Clifford circuits as unitary 2-design	S1
A. Frame potential	S1
B. Numerical algorithm	S2
C. Numerical results	S4
S2. Detailed numerical simulation results for the entanglement growth	S4
S3. Detailed numerical simulation results for the phase transition	S5
References	S6

S1. RANDOM CLIFFORD CIRCUITS AS UNITARY 2-DESIGN

One of the main results of our work relies on the decoupling inequality, which requires that the set of random unitaries to be averaged over forms a unitary 2-design. While it is well-known that the n -qubit Clifford group forms a unitary 2-design [1], it is yet to be verified that an ensemble of random quantum circuits of depth d made out of 2-qubit Clifford gates also approximates a unitary 2-design for n qubits. In this section, we numerically compute the frame potential for such unitary circuits, which quantifies the extent to which it approximates unitary designs. Our results confirm that the ensemble of depth d circuits of local 2-qubit Clifford gates indeed approximates a unitary 2-design when d is large. In what follows, we first review the frame potential, introduce our algorithm to compute it, and then present numerical results.

A. Frame potential

The k -th frame potential of a unitary ensemble ν is defined by

$$F_\nu^{(k)} = \frac{1}{|\nu|^{2k}} \sum_{U, V \in \nu} |\text{tr}(U^\dagger V)|^{2k}, \quad (\text{S1})$$

where $|\nu|$ denotes the order of the ensemble. One of the nice properties of the k -th frame potential $F_\nu^{(k)}$ is that this quantity is minimized when the unitary ensemble is drawn from the Haar measure (in which the summation in Eq. (S1) is replaced by integration):

$$F_\nu^{(k)} \geq F_{\mu_{\text{Haar}}}^{(k)} = k!. \quad (\text{S2})$$

Furthermore, it is well known that the k -th frame potential saturates this lower bound if and only if the unitary ensemble ν forms a unitary k -design [2]. Therefore, by explicitly computing the second frame potential $F_\nu^{(2)}$, we can verify if the ensemble of Clifford circuits forms an approximate 2-design.

* SC and YB contributed equally to this work.

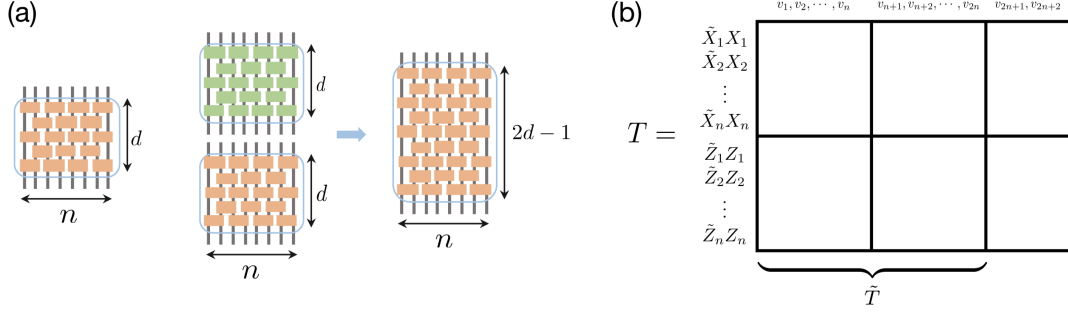


FIG. S1. (a) Left: the layout of the random Clifford circuit U considered in this work. For a pair of circuits U and V drawn from an ensemble ν_d of depth d circuits, $U^\dagger V$ is, equivalently, a unitary drawn from ν_{2d-1} of depth $2d-1$. (b) An illustration of matrix T . The first and the second n rows of T represent operators $\tilde{X}_1 X_1, \dots, \tilde{X}_n X_n$ and $\tilde{Z}_1 Z_1, \dots, \tilde{Z}_n Z_n$, respectively. Each operator is specified by using a length $2n+2$ binary vector, based on the Eq. (S5).

B. Numerical algorithm

While it is well known that the unitary evolution of a quantum state under Clifford gates can be efficiently simulated using classical computers [3–6], this does not imply that one can explicitly evaluate the matrix that implements the unitary time evolution. Computing the exact frame potential for an ensemble of Clifford circuits is a formidable task mainly due to two reasons. First, in a naïve approach, taking the trace of a Clifford unitary requires simulating the evolution of exponentially many different initial states owing to the large Hilbert space. Second, the summation over every element, U, V , from the ensemble of random Clifford circuit is computationally expensive due to the large size of the ensemble. While the second difficulty can be resolved by performing Monte Carlo sampling of the group elements, the first challenge is non-trivial.

In this section, we provide an efficient algorithm to compute the trace of a Clifford circuit. In comparison to the naïve approach of simulating the evolution of exponentially many different initial states, our approach takes only a polynomial time as a function of system size n .

Recall that the k -th frame potential for an ensemble of Clifford circuits of depth d is of the form

$$F_{\nu_d}^{(k)} = \frac{1}{|\nu_d|^2} \sum_{U, V \in \nu_d} |\text{tr}(U^\dagger V)|^{2k}. \quad (\text{S3})$$

Here, we focus on the layout of the circuit shown in Fig. S1a, while our technique introduced here is more broadly applicable. Since both U and V consist of d layers of random Clifford gates, we note that $U^\dagger V$ can be also regarded as a circuit of depth $2d-1$ without loss of generality. Therefore, we can rewrite the frame potential as

$$F_{\nu_d}^{(k)} = \frac{1}{|\nu_{2d-1}|} \sum_{U \in \nu_{2d-1}} |\text{tr} U|^{2k} = \frac{1}{|\nu_{2d-1}|} \sum_{U \in \nu_{2d-1}} |\text{tr} U \text{tr} U^\dagger|^k = \frac{1}{|\nu_{2d-1}|} \sum_{U \in \nu_{2d-1}} |Q_U|^k, \quad (\text{S4})$$

where $Q_U \equiv \text{tr} U \text{tr} U^\dagger$. Thus, our problem reduces to computing Q_U exactly for a given unitary U , and then performing a Monte-Carlo sampling of U over different realizations of the depth $2d-1$ random Clifford circuits. Below, we focus on the computation of Q_U assuming U is given as a Clifford circuit.

Our key idea is to further simplify the expression Q_U using Pauli operators. In particular, we are interested in evaluating Q_U without having to explicitly construct the unitary matrix U . This is in fact possible, because, by the definition of the Clifford group, the unitary U can be fully characterized by specifying how generators of n -qubit Pauli group \mathcal{P} transform under the conjugation by U [7]. To this end, it is important to introduce an efficient notation to denote a Pauli element. Here and below, we adapt and extend the notation for Pauli operators in the existing literature [7] and denote an element in the n -qubit Pauli group by a binary string $v = v_1 v_2 \dots v_{2n+2}$ of length $2n+2$:

$$P_v = (-1)^{v_{2n+1} i^{v_{2n+2}}} \prod_{j=1}^n K_j(v_j, v_{j+n}), \quad (\text{S5})$$

where $K_j(1,0) = X_j$, $K_j(0,1) = Z_j$, or $K_j(1,1) = Y_j$ represents one of the Pauli operators for a qubit at site j , following the convention in [7]. In other words, the first $2n$ bits in a string v specify the n -qubit Pauli string, and the last two digits control the overall coefficient. We will find that the global prefactor $(-1)^{v_{2n+1} i^{v_{2n+2}}}$ is often not very

important other than that it gives rise to exactly four elements in \mathcal{P} per a single Pauli string (with different prefactors). Hence, for notational brevity, we denote the first $2n$ bits of v as $\bar{v} = v_1 v_2 \dots v_{2n}$. In this way, the product of two Pauli strings can be concisely represented as a simple XOR operation on corresponding binary strings: if $P_v \equiv P_u P_w$, then $\bar{v} = \bar{u} + \bar{w}$, where the “+” operator should be interpreted as element-wise XOR operations. This establishes the one-to-one correspondence between a binary string of length $2n$ and every group element in \mathcal{P} up to a prefactor. In particular, the group multiplication in \mathcal{P} corresponds to a linear operation in the binary string. Furthermore, the set of binary strings forms a vector space with respect to XOR operations. We note that the prefactor of v can be also computed from u and w .

In order to compute Q_U , we first re-express it using the fact that the Pauli group \mathcal{P} forms a unitary 1-design. More specifically, for any n -qubit operator O , we have, $\text{tr}(O) \cdot \mathbb{1} = \frac{1}{4D} \sum_{P \in \mathcal{P}} P O P^\dagger$. Then, it follows:

$$Q_U = \text{tr} U^\dagger \text{tr} U = \text{tr}(U^\dagger \mathbb{1} \cdot \text{tr}(U)) = \frac{1}{D} \sum_{P \in \mathcal{P}^+} \text{tr}(U^\dagger P U P^\dagger) = \frac{1}{D} \sum_{P \in \mathcal{P}^+} \text{tr}(\tilde{P} P^\dagger), \quad (\text{S6})$$

where $D = 2^n$ is the Hilbert space dimension, $\tilde{P} \equiv U^\dagger P U$, and the summation is over the operators in the set $\mathcal{P}^+ = \{\mathbb{1}, X, Y, Z\}^{\otimes n}$, ignoring the irrelevant complex prefactor (which cancels the factor $1/4$). We note that $\tilde{P} P^\dagger$ is also a Pauli operator and its trace is non-vanishing if and only if $\tilde{P} P^\dagger \propto \mathbb{1}$. Therefore, in order to evaluate Q_U , we only need to count how many $P \in \mathcal{P}^+$ gives rise to a non-vanishing contribution. We denote the set of such Pauli operators as \mathcal{K}_U .

Our key observation is that \mathcal{K}_U is closed under multiplications to form a subgroup of \mathcal{P} , and its binary representation form a linear vector space over binary field. Therefore, counting the number of element in \mathcal{K}_U can be efficiently achieved by computing the dimension of the vector space \mathcal{K}_U . Here and below, we use the same notation \mathcal{K}_U to refer to both the vector space and the subgroup of Pauli group whenever there is no ambiguity. Below, we will discuss some important properties of \mathcal{K}_U . In particular, we will demonstrate that the computation of Q_U always falls into one of three cases:

- \mathcal{K}_U contains only the identity operator. Namely, the Pauli operator P satisfies $\tilde{P} P^\dagger \propto \mathbb{1}$ only when $P = \mathbb{1}$. $Q_U = 1$;
- \mathcal{K}_U of dimension N is generated by N Pauli operators P with $\tilde{P} P^\dagger = \mathbb{1}$. \mathcal{K}_U contains 2^N Pauli operators, $Q_U = 2^N$;
- There exists at least one generator P of \mathcal{K}_U satisfying $\tilde{P} P^\dagger = -\mathbb{1}$. Then, there are equal numbers of Pauli operators P with $\tilde{P} P^\dagger = \mathbb{1}$ and P with $\tilde{P} P^\dagger = -\mathbb{1}$, i.e., the operators satisfying $\tilde{P} P^\dagger = \mathbb{1}$ and $-\mathbb{1}$ come in pairs. $Q_U = 0$.

To see this, we notice that, for any $P_v \in \mathcal{P}$, $\text{tr}(\tilde{P}_v P_v^\dagger)$ is always real since

$$\text{tr}(\tilde{P}_v P_v^\dagger)^* = \text{tr}(U^\dagger P_v U P_v^\dagger)^* = \text{tr}(P_v U^\dagger P_v^\dagger U) = (-1)^{2v_{2n+2}} \text{tr}(P_v^\dagger U^\dagger P_v U) = \text{tr}(\tilde{P}_v P_v^\dagger). \quad (\text{S7})$$

This implies $\text{tr}(\tilde{P}_v P_v^\dagger) \neq 0$ if and only if $\tilde{P}_v P_v^\dagger = \pm \mathbb{1}$. We use \mathcal{K}_U^\pm to denote the set of operators P_v satisfying $\tilde{P}_v P_v^\dagger = \pm \mathbb{1}$, respectively. \mathcal{K}_U^+ forms a normal subgroup of \mathcal{K}_U . If \mathcal{K}_U^- is trivial, i.e., contains no element, \mathcal{K}_U^+ is exactly \mathcal{K}_U . When \mathcal{K}_U^- is non-trivial, we require at least one generator P of \mathcal{K}_U satisfies $\tilde{P} P^\dagger = -\mathbb{1}$. In this case, \mathcal{K}_U^+ becomes the maximal normal subgroup of \mathcal{K}_U , and the quotient group $\mathcal{K}_U / \mathcal{K}_U^+ = \mathbb{Z}/2\mathbb{Z}$. Therefore, \mathcal{K}_U^\pm contain the same number of elements, and, as a result, $Q_U = 0$.

Due to this correspondence between P satisfying the property $\tilde{P} P^\dagger \propto \mathbb{1}$, and the linear space \mathcal{K}_U , counting the number of such operators can be efficiently accomplished by finding out a set of mutually commuting generators of the group, or, equivalently, the basis of the linear space \mathcal{K}_U in the binary representation. Namely, the number of elements in \mathcal{K}_U is given by $2^{m_\mathcal{K}}$, where $m_\mathcal{K}$ is the dimension of \mathcal{K}_U . In the second case where all operators P in \mathcal{K}_U satisfy $\tilde{P} P^\dagger = \mathbb{1}$, $Q_U = 2^{m_\mathcal{K}}$.

Now, the calculation of Q_U reduces to figuring out $m_\mathcal{K}$ and the existence or the absence of any generator P satisfying $\tilde{P} P^\dagger = -\mathbb{1}$. In order to find out $m_\mathcal{K}$, we introduce a matrix T of size $2n$ by $2n+2$. The first and the second n rows of T represent the Pauli operators $\tilde{X}_i X_i$ and $\tilde{Z}_i Z_i$, respectively (see Fig. S1b). We denote the first $2n$ columns of T by \bar{T} . Since the identity operator $\mathbb{1} \in \mathcal{P}$ corresponds to the zero in the binary representation, one can easily check that the linear space \mathcal{K}_U can be determined from the kernel of \bar{T} (over the binary field). Furthermore, one can determine the sign of $\tilde{P}_\alpha P_\alpha$ for every basis vector in \mathcal{K}_U by explicitly performing the effective “Gaussian elimination” (or row operations) that properly accounts for the changes in the prefactors of Pauli operators. Motivated from Ref. [7], we define a modified *rowsum()* function. The *rowsum()* function takes two rows of T (corresponding to operators $\tilde{P}_u P_u^\dagger$ and $\tilde{P}_v P_v^\dagger$) as input and returns a binary representation for the operator $\tilde{P}_v \tilde{P}_u P_u^\dagger P_v^\dagger$:

$$\text{rowsum}(\tilde{P}_u P_u^\dagger, \tilde{P}_v P_v^\dagger) = \tilde{P}_v \tilde{P}_u P_u^\dagger P_v^\dagger = (-1)^{-i \Lambda_n \bar{v}} \tilde{P}_v P_v P_u P_u^\dagger, \quad (\text{S8})$$

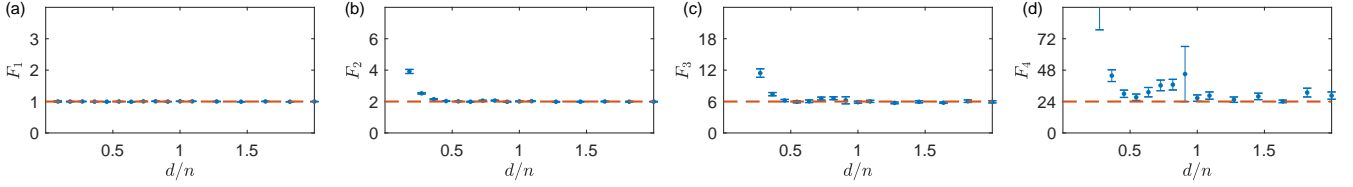


FIG. S2. Numerical computation of the first, second, third, and fourth frame potentials (from (a) to (d)) as a function of circuit depth $2 \leq d \leq 44$ for system size $n = 22$ qubits. The frame potentials are estimated from 50000 randomly generated Clifford circuits. The depths of circuit d is taken from 2 to 44 (blue markers). Orange dashed lines represent the corresponding values for the Haar random unitary ensemble.

where $P_t = \tilde{P}_u P_u^\dagger$, and $\Lambda_n = [0, \mathbb{1}_n; -\mathbb{1}_n, 0]$ is the symplectic form. By checking the value in the $(2n + 1)$ -th column, we can determine the sign for generators $\tilde{P}_v P_v$ of the kernel \mathcal{K}_U . In this way, we can compute Q_U for each realization of the circuit and further obtain the frame potential.

C. Numerical results

The results of our numerical calculations are summarized in Fig. S2, which shows that, the first, second, and third frame potentials for the random Clifford circuit ensemble approach to corresponding values for a unitary 1, 2 and 3-design when the depth of circuit d is sufficiently large, $\sim O(n)$, as predicted in [8]. In contrast, the fourth frame potential significantly deviates from the value for a unitary 4-design, which is expected since it has been proved that even the n -qubit Clifford group does not form a unitary 4-design [9].

In the model proposed in the main text, each cluster consists of $m = 11$ qubits, hence a nearest neighboring cluster pair have total $n = 2m = 22$ qubits. Our numerical results in Fig. S2b indicate that random Clifford circuits of depth $d = 44$ are sufficient to approximate a unitary 2-design in such a case.

S2. DETAILED NUMERICAL SIMULATION RESULTS FOR THE ENTANGLEMENT GROWTH

Figure S3 provides detailed information on the entanglement growth and saturation in various parameter regimes. We focus on two different values of the local circuit depth, $d = 3$ or 44 , and simulate the quantum dynamics for various values of the measurement fraction p . When $d = 3$, each local circuit fails to approximate a unitary 2-design, and quantum information cannot be fully scrambled even within the local Hilbert space of a m -qubit box. In this regime, the growth of entanglement entropy can be significantly affected by random projective measurement. Indeed, we find that the projective measurements reduce the half-chain entanglement starting from the early time evolution at $t = 0$. Also, the steady state entanglement entropy per qubit stays outside the triangle defined by $1 - 2p$ and $1 - p$ as shown in Fig. 2d in the main text.

In contrast, when $d = 44$, each Clifford unitary U approximates a unitary 2-design for $2m = 22$ qubits as demonstrated in the previous section. One can apply the decoupling inequality as discussed in the main text, leading to two nontrivial predictions. First, the saturation of entanglement entropy per qubit should lie between $1 - 2p$ and $1 - p$. Second, during early time evolution, the entanglement entropy should not be significantly decreased by projective measurements as long as $\gamma < 1 - 2p$, where γ is the entanglement entropy per qubit. This regime, referred to as QEC regime below, is indicated by using a vertical line with the identification $\gamma = S/(Lm/2)$. Strictly speaking, this identification is not exact, since the relevant γ for decoupling theorem is obtained from the entanglement entropy between a neighboring qubit blocks and the rest of the system, rather than from the half-chain entanglement S . Still, we expect the qualitatively similar behavior. Our expectation is explicitly verified in Fig. S3e and Fig. S3f, where $\Delta S_{meas} \approx 0$ within errorbars. We also notice that the entanglement reduction remains small even beyond the QEC regime. When $p > 0.5$, the inequality $\gamma < 1 - 2p$ cannot be satisfied by any finite positive γ , in which case projective measurements may reduce the entropy during the early time evolution starting from $t = 0$. While our argument based on the decoupling inequality for the stability of the volume-law phase cannot be applied in this regime, our numerical simulations suggest that the volume-law phase may still persist at least up to $p \lesssim 0.89$ with a sufficiently large d .

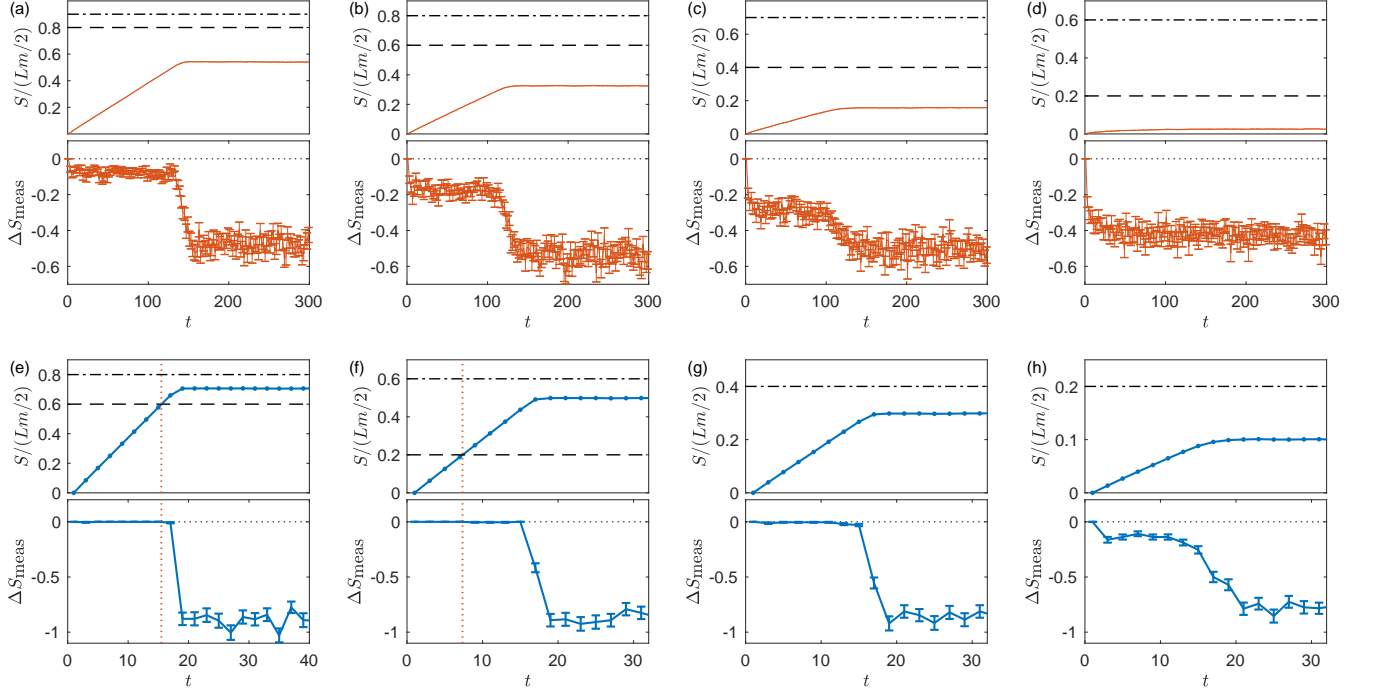


FIG. S3. Half-chain entanglement dynamics in various parameter regimes. Simulations are performed for systems with $L = 32$, $m = 11$. Upper panels in (a-h): the growth of entanglement entropy per qubit as a function of time t . Black dashed lines indicate $1 - 2p$, which correspond to the maximum γ for which the decoupling inequality can be applied. Black dash-dotted lines indicate $1 - p$, which correspond to the maximum possible entanglement entropy per qubit after projective measurements. Lower panels in (a-h): the change of entanglement entropy before and after random projective measurements in each time step. The errorbars represent the variance of entanglement reduction by measurements. (a-d): The depth of the local Clifford circuit $d = 3$, and the measurement fraction is $p = 0.1, 0.2, 0.3, 0.4$, respectively (from left to right). (e-h): The depth of the local Clifford circuit $d = 44$, and $p = 0.2, 0.4, 0.6, 0.8$, respectively (from left to right). In this regime, the local circuit approximates a unitary 2-design. The red dotted vertical lines in (e) and (f) indicate when the entanglement entropy per qubit, $S/(Lm/2)$, exceeds the condition for the decoupling theorem ($\gamma < 1 - 2p$). All the results in this figure are averaged over 240 different realizations of the random unitary circuit.

S3. DETAILED NUMERICAL SIMULATION RESULTS FOR THE PHASE TRANSITION

In this section, we present the full numerical simulation results for the entanglement phase transition, including both the critical points (d_c, p_c) and critical exponents. Following the entanglement scaling hypothesis proposed in a recent work [10], we perform a finite-size scaling analysis with the scaling ansatz:

$$S(p, L) = \alpha \ln L + \mathcal{F}\left((p - p_c)L^{1/\nu}\right), \quad (\text{S9})$$

where α is a constant, characterizing the logarithmic entropy at the critical point, p_c is the critical measurement fraction, ν is the correlation length critical exponent, and $\mathcal{F}(x)$ is a universal function. We expect that the universal function $\mathcal{F}(x)$ takes the following qualitative behaviors:

$$\mathcal{F}(x) \approx \begin{cases} |x|^\nu & (x \rightarrow -\infty) \\ \text{const.} & (x = 0) \\ -\alpha\nu \ln x & (x \rightarrow \infty). \end{cases} \quad (\text{S10})$$

Thus, in the thermodynamic limit $L \rightarrow \infty$, when $p > p_c$, $S(p, L)$ converges to a constant with no dependence on L , indicating the area-law phase. In the case $p < p_c$, $S(p, L)$ scales linearly in L with a log correction. In practice, we subtract the entropy at the critical point, $\alpha \ln L$, (with numerically optimized p_c) from both sides of Eq. (S9), converting it into a conventional finite size scaling form [10], i.e.,

$$S(p, L) - S(p_c, L) = \mathcal{F}\left((p - p_c)L^{1/\nu}\right). \quad (\text{S11})$$

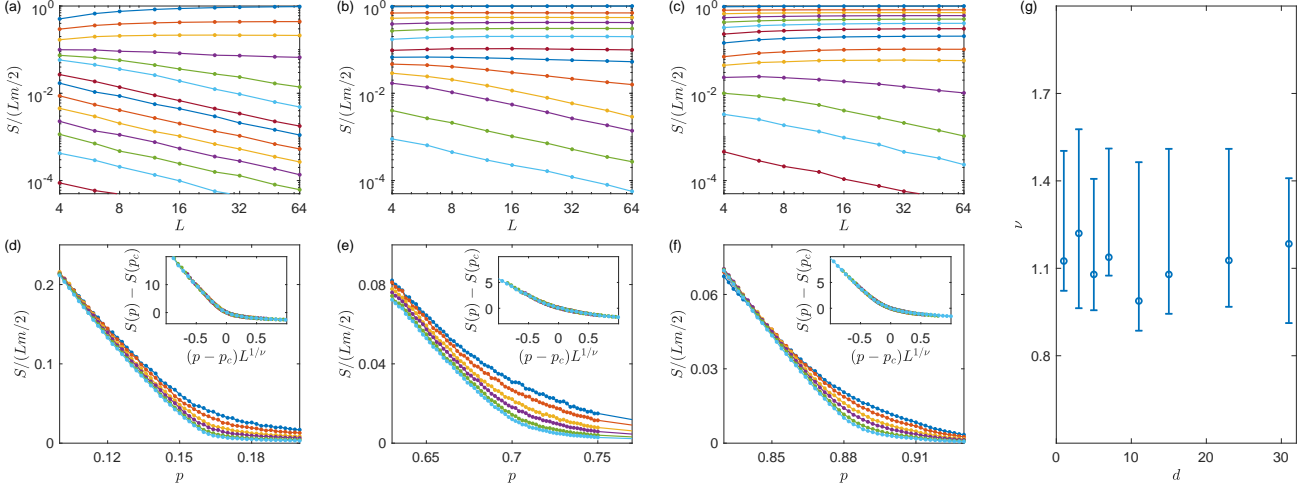


FIG. S4. Finite size scaling analysis and critical exponents. (a-c) The entanglement density $S/(Lm/2)$ as a function of system size L for different depths of local circuits, $d = 1, 7, 31$, respectively (from left to right). Different curves correspond to our numerical results with different measurement fractions. System size L ranges from 4 to 64. (d-f) The entanglement density as a function of measurement fraction for $d = 1, 7, 31$, respectively (from left to right). Different curves correspond to results from different system sizes $L = 12, 16, 24, 32, 48, 64$. Data collapses are presented in the insets using the scaling hypothesis Eq. S9. (g) Numerically extracted critical exponents ν for different values of d . We estimate the errorbars for ν by the minimized cost function Q for different choices of p_c .

d	1	3	5	7	11	15	23	31
ν	1.13	1.22	1.08	1.14	0.99	1.08	1.13	1.18
p_c	0.16	0.41	0.59	0.71	0.83	0.86	0.88	0.89

TABLE SI. Critical exponents ν and critical points p_c for random Clifford circuits with different depths d of local circuit. We use the scaling hypothesis that considers a log correction to the volume law phase. The number of qubits in a cluster $m = 11$. The error bars for ν are given in Fig. S4g.

More specifically, we numerically optimize the parameter p_c and ν by minimizing the cost function

$$Q = \frac{1}{N} \sum_{i,j} \frac{(y_{ij} - Y_{ij})^2}{dy_{ij}^2 + dY_{ij}^2}, \quad (\text{S12})$$

where Y_{ij} , dY_{ij} are the values given by the scaled function and its standard error at x_{ij} , and y_{ij} , dy_{ij} are the data points at x_{ij} . The index j labels different system sizes and i labels different measurement fractions. The detailed algorithm can be found in [11, 12]. Our finite size scaling analysis and numerically extracted parameters, ν and p_c , are summarized in Tab. SI and Fig. S4. Our results suggest that the critical exponent ν takes a universal value ~ 1.1 , independent of d .

-
- [1] D. P. DiVincenzo, D. W. Leung, and B. M. Terhal, IEEE Transactions on Information Theory **48**, 580 (2002).
[2] D. A. Roberts and B. Yoshida, Journal of High Energy Physics **2017**, 121 (2017).
[3] C. H. Bennett, D. P. DiVincenzo, J. A. Smolin, and W. K. Wootters, Physical Review A **54**, 3824 (1996).
[4] A. R. Calderbank, E. M. Rains, P. W. Shor, and N. J. Sloane, Physical Review Letters **78**, 405 (1997).
[5] D. Gottesman, Physical Review A **54**, 1862 (1996).
[6] D. Gottesman, arXiv preprint quant-ph/9807006 (1998).
[7] S. Aaronson and D. Gottesman, Physical Review A **70**, 052328 (2004).
[8] F. G. Brandao, A. W. Harrow, and M. Horodecki, Communications in Mathematical Physics **346**, 397 (2016).
[9] Z. Webb, arXiv preprint arXiv:1510.02769 (2015).
[10] Y. Li, X. Chen, and M. Fisher, arXiv preprint arXiv:1901.08092 (2019).
[11] J. Houdayer and A. K. Hartmann, Physical Review B **70**, 014418 (2004).
[12] N. Kawashima and N. Ito, Journal of the Physical Society of Japan **62**, 435 (1993).